Alq_3 coated silicon nanomembranes for cavity optomechanics

F. Fogliano[a], A. Ortu[a], A. Camposeo[b], D. Pisignano[b,c], D. Ciampini[a,d], F. Fuso[a,d], and E. Arimondo[a,d]

[a]Dipartimento di Fisica "E. Fermi", Università di Pisa, Largo Bruno Pontecorvo 3, I-56127 Pisa, Italy
[b]Istituto Nanoscienze-CNR, Euromediterranean Center for Nanomaterial Modelling and Technology (ECMT), via Arnesano I-73100, Lecce, Italy
[c]Dipartimento di Matematica e Fisica Ennio De Giorgi, Università del Salento, via Arnesano I-73100 Lecce, Italy
[d]INO-CNR, Via G. Moruzzi 1, I-56124 Pisa, Italy

ABSTRACT

The optomechanical properties of a silicon-nitride membrane mirror covered by Alq_3 and Silver layers are investigated. Excitation at two laser wavelengths, 780 and 405 nm, corresponding to different absorptions of the multilayer, is examined. Such dual driving will lead to a more flexible optomechanical operation. Topographic reconstruction of the whole static membrane deformation and cooling of the membrane oscillations are reported. The cooling, observed for blue laser detuning and produced by bolometric forces, is deduced from the optomechanical damping of the membrane eigenfrequency. We detemine the presence of different contributions to the photothermal response of the membrane.

Keywords: Cavity optomechanics, photothermal forces, multilayer medium.

1. INTRODUCTION

The optomechanical handling of objects is a very active research area, as presented in the review by Aspelmeyer et al.[1] Since the object dimensions can span from the nanoscale to macroscopic scales, the corresponding range of applications is very wide, including quantum computation with optomechanically coupled hybrid qubits, as well as macroscopic motion control such as in gravitational wave detection. In this framework, a significant effort is associated to looking for new materials and new optomechanical processes. The basic mechanism of optomechanics is the exchange of momentum between photons and the controlled material[2,3] . Experiments with dielectric membranes or metal/dielectric bilayers were instead based on photothermal processes, i.e. on membrane deformation by laser heating[4] . In a recent experiment by Usami et al.,[5] the motion of a thin GaAs semiconductor membrane was laser cooled to near zero absolute temperature through the coupling to a low finesse cavity. As striking novelty the source of the optomechanical coupling was provided by photo-excited excitons whose nonradiative decay leads to heating and deformation of the membrane.

The present work investigates the optomechanical properties of the molecular organic semiconductor tris(8-hydroxyquinoline) aluminum (Alq_3) as a thin film[6] . This material has been widely investigated for its optical applications[7,8] . Owing to its luminescence, charge transport and energy transfer properties, and low cost, this compound is used in many optoelectronic devices such as photodetectors, organic LEDs, lasers, etc.. An optomechanical investigation would further increase the application range of the material.

Our study is based on a cavity containing a fixed mirror and a multilayer membrane composed by silicon-nitride coated with Alq_3 and also silver in order to increase the reflectivity. As in the previous study on GaAs[5] the cavity has a low finesse to enhance the optomechanical coupling produced by photothermal and possibly by direct electronic processes. We study the optomechanical response for two different wavelengths, one centred

Send correspondence to Ennio Arimondo E-mail: ennio.arimondo@unipi.it
A.C: E-mail: andrea.camposeo@cnr.it
D.C: E-mail: donatella.ciampini@unipi.it

Optical Trapping and Optical Micromanipulation XIII, edited by Kishan Dholakia, Gabriel C. Spalding, Proc. of SPIE Vol. 9922, 99220G · © 2016 SPIE · CCC code: 0277-786X/16/$18 · doi: 10.1117/12.2235276

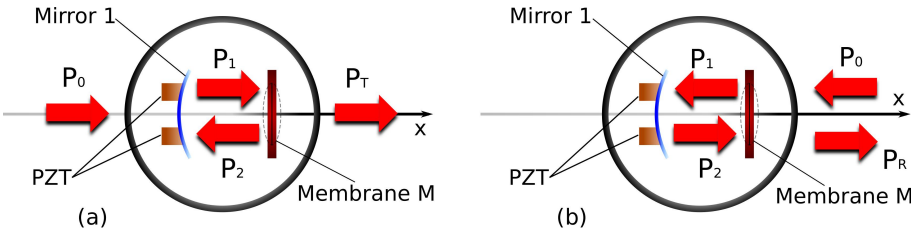

Figure 1. Cavity configurations with P_{in} laser input power entering from left, in (a), and from right in **(b)**. P_1 and P_2 **are** the intracavity powers, and P_T, P_R the transmitted and reflected powers whose forces act on the membrane.

within the Alq_3 absorption band and a second one outside that band in order to isolate the optomechanical contribution of that material.

Our optomechanic apparatus has a few original features. Since the forces on an intracavity membrane depend on the photon injection side, we compare the optomechanical response by switching the cavity input. This flexibility might enhance the overall control on optomechanical devices. We perform a local optical-lever measurement of the membrane deformation. By scanning the probe laser on the membrane, we perform a topographic reconstruction of the deformation. We apply these experimental tools to probe either Alq_3-coated or pristine membranes, in order to define the photothermal contributions from the organic material or from the silver coating.

Section 2 recalls the basic equations describing the optomechanical processes linking the amplitude and sign of the optomechanical forces to the macroscopic properties of the cavity. The role of the different forces, static and time-dependent (dynamic), is emphasized for a connection to the experimental observations. Section 3 discusses the characteristic of the experimental apparatus, and Section 4 examines the membrane optical properties. Section 5 presents the experimental results, from the photothermal frequency response, to the topographic reconstruction, and to the membrane cooling. The discussion and conclusion Section completes our work. An Appendix contains the cavity geometrical parameters determining the radiative or bolometric forces.

2. FORCES AND MEMBRANE MOTION

2.1 Cavity and membrane

We consider a cavity with length L composed by the mirror 1 and the membrane M as in Fig. 1. The cavity properties are determined by the reflectivity, absorption and transmission for the mirror and the membrane. The not-absorbing mirror has intensity reflection coefficient R_1 and transmission $T_1 = 1 - R_1$. The absorbing multilayer membrane is characterized by electric field reflectivity r_M and transmittivity t_M, complex quantities including an electric field phase shift as in the Appendix. The R_M power reflection and $T_M$power transmission coefficients are linked to the electric field parameters as $R_M = |r_M|^2$ and $T_M = |t_M|^2$. For an absorbing medium notice that $R_M + T_M \neq 1$.

The main cavity parameter is the finesse $\mathcal{F}$ given by[9]

$$\mathcal{F} = \frac{\pi \left(R_1 R_M\right)^{1/4}}{1 - \sqrt{R_1 R_M}}. \tag{1}$$

The membrane displacement ΔL modifying the cavity length is produced by the total applied force F with an equation of motion given by

$$\frac{\partial^2}{\partial t^2}\Delta L + \gamma_M \frac{\partial}{\partial t}\Delta L + \omega_M^2 \Delta L = \frac{F}{m} \tag{2}$$

where γ_M is the mechanical damping coefficient, ω_M the oscillation frequency and m the membrane mass.

2.2 Static forces

The laser light at frequency ω_L may enter into the cavity either from the mirror 1 on the left of Fig. 1 (configuration denoted as L left), or from the membrane side (R right configuration). The two configurations produce

different forces on the membrane to be denoted as F_L and F_R, respectively. The radiation pressure force, F^{rad}, determined by the momentum carried by each photon reaching the membrane, is given by the power divided by the light speed for each impinging laser beam[10] . For a given input power, P_{in}, the L and R configurations lead to the following forces on the membrane

$$\begin{aligned} F_L^{rad} &= \frac{1}{c}(P_1 + P_2 - P_T), \\ F_R^{rad} &= \frac{1}{c}(P_2 + P_1 - P_{in} - P_R). \end{aligned} \tag{3}$$

Using the equations for the light propagation inside the cavity and taking into account that the cavity length is modified by the ΔL membrane displacement[1] , these forces are written as

$$F_{(L,R)}^{rad} = c_{(L,R)}^{rad} \frac{2\mathcal{F}/\pi}{1 + \left[\frac{2}{\kappa}(\delta\omega + g\Delta L)\right]^2} \frac{P_{in}}{c}, \tag{4}$$

where $\delta\omega = \omega_L - \omega_c$ with ω_c the cavity resonance frequency, $\kappa = \pi c/(\mathcal{F}L)$ the cavity damping, and $g = \omega_c/L$ the optomechanics coupling constant. The force is enhanced by the cavity finesse, with a correction term, the $c_{L,R}^{rad}$ geometrical parameter, depending on the specific cavity (L,R) geometry. These parameters, with expressions within the Appendix, are smaller than 1.

The photon-induced forces, denoted as bolometric or photothermal forces[11] , are produced by the absorbed light. For our multilayer system the absorption produced by both Silver and Alq_3 films should be considered. The absorption is associated to the intracavity power and we introduce a Λ^{tot} parameter describing the ratio between the bolometric and radiative forces on our system, the total superscript recalling the combined action of Ag and Alq_3. In addition we introduce the $c_{L,R}^{bol}$ geometrical parameters analogous to the radiative ones depending on the the specific cavity (L,R) geometry and whose expressions are also in the Appendix. In analogy to Eq. (4) our membrane bolometric force results

$$F_{(L,R)}^{bol} = c_{(L,R)}^{bol} \Lambda^{\mathrm{tot}} \frac{2\mathcal{F}/\pi}{1 + \left[\frac{2}{\kappa}(\delta\omega + g\Delta L)\right]^2} \frac{P_{in}}{c}, \tag{5}$$

The present definition of the Λ^{tot} parameters, different from the original one[11] , separates the contribution of the cavity geometry given by the c^{bol} parameters from the physics of the photothermal process.

In a static regime, the above forces produce a static membrane deformation ΔL^{st} that for $\delta\omega = 0$ and within the linear regime response is given by

$$\Delta L^{ss} = \left(c_{L,R}^{rad} + c_{(L,R)}^{bol}\Lambda^{tot}\right) \frac{2\mathcal{F}}{\pi m \omega_M^2} \frac{P_{in}}{c}. \tag{6}$$

For large values of the applied force corresponding to $\Delta L \geq L\kappa/\omega_c$[1] , the nonlinear temporal dynamics associated to the membrane motion and the cavity field propagation leads to the occurrence of self-oscillations[11–13] at the following frequency:

$$\omega^{so} = \omega_M \sqrt{\frac{\kappa}{\kappa + \gamma_M}\left[1 + \frac{\kappa}{Q_M \omega_M}\left(\frac{1}{4} + \frac{g^2\left(\Delta L^{ss}\right)^2}{\kappa^2}\right)\right]} \tag{7}$$

In our case the correction term under the square root is around three percent, and therefore $\omega^{so} \approx \omega_M$.

2.3 Dynamic forces

In presence of time-dependent forces, or while monitoring the membrane dynamic evolution, the finite time response of the forces plays an essential role. Refs.[4,14] have introduced the τ_c time time response directly into the radiative or bolometric force as

$$F^{bol} = \int_{-\infty}^{t} dt' \frac{\partial F(L(t'))}{\partial t'}\left(1 - e^{-(t-t')/\tau_c}\right) = \int_{-\infty}^{t} dt' \nabla F \frac{\partial L(t')}{\partial t'}\left(1 - e^{-(t-t')/\tau_c}\right), \tag{8}$$

with the ∇F force rigidity given by

$$\nabla F = \frac{\partial F(L)}{\partial L} \tag{9}$$

The rigidity calculated as the derivative of Eq. (4) or (5) is zero at the cavity resonance and takes maximum values with opposite signs, at half-linewidth blue or red laser detunings. The rigidity approach is very convenient when considering the oscillating motion of the membrane at a given frequency, for instance ω_M. Then, the integral of Eq. (8) is easily performed and the motion is determined by the following effective damping and spring constants[11] :

$$\begin{aligned} \gamma_M^{eff} &= \gamma_M \left(1 + \frac{\omega_M^2 \tau_c}{\gamma_M} \frac{1}{1+\omega_M^2\tau_c^2} \frac{\nabla F}{m\omega_M^2}\right) \\ (\omega_M^{eff})^2 &= \omega_M^2 \left(1 - \frac{1}{1+\omega_M^2\tau_c^2} \frac{\nabla F}{m\omega_M^2}\right). \end{aligned} \tag{10}$$

The previous formulas lead to an effective temperature T^{eff} for the membrane oscillation frequency. With T the starting temperature (room temperature in our case), the optomechanical action leads, for small frequency shifts $\omega_M^{eff} \approx \omega_M$, to the following T^{eff}[15] :

$$T^{eff} = T \frac{\gamma_M}{\gamma_M^{eff}}. \tag{11}$$

3. EXPERIMENTAL SETUP

Our apparatus, schematically shown in Fig. 2 a) is based on a hemiconfocal cavity with $L = 25$ mm length and 6 GHz FSR. The silica spherical mirror has $R_1 = 0.997$ reflectivity. The mirror position is controlled by piezoelectrics allowing us to vary the cavity length and to scan the cavity resonances at fixed laser frequency. The plane membrane shown in Fig. 2b and forming the second mirror is a silicon-nitride thin film, with thickness 50 nm or 100 nm and low tensile stress, < 250 MPa. The membrane has an area of 1 mm^2, clamped to a silicon squared frame of 7.5 mm. Two different layers are deposited onto the membrane: a 20 nm thick organic semiconductor film (Alq_3) and a 60 nm thick Silver coating enhancing the reflectivity. Focusing on photothermal effects, we locate the organic layer within the cavity in order to maximize its absorption of the laser radiation. The multilayer reflectivity is $\approx 90\%$ for the infrared laser, which corresponds to a cavity finesse $F \approx 80$, and $\approx 80\%$ for the blue laser, which corresponds to a cavity finesse $F \approx 25$. A 100 nm thickness membrane without the Alq_3 layer is used for reference. The cavity system is placed inside a vacuum chamber at a pressure $\approx 2 \cdot 10^{-6}$ mBar.

The cavity is excited by two different pump lasers, corresponding to two different absorption rates of Alq_3: a 780 nm infrared laser diode, frequency-stabilized on an Rb atomic absorption line, and a blue laser diode at the 405 nm wavelength, centred on the absorption of the organic material. The lasers are focused on the membrane in order to optimize the mode matching with the optical cavity through a beam waist of 79μm$\times 57$ μm. The laser input power is controlled via an acousto-optic modulator. Owing to the optical design we perform optomechanics measurements in both the L/R configurations schematized in Fig. 1.

A He-Ne laser probes the membrane displacement using an optical lever with one meter arm and a four-quadrant split photodiode. The reflected beam detection by a 250 kHz bandwidth four-quadrant sensor probes the membrane deformation along two orthogonal directions. By tuning through XY micrometric controls the incidence position of the probe laser on the membrane, a topography reconstruction of the membrane spatial profile is obtained. Best topographic signals are collected with 0.2 mW power and by a 50 μm diameter spot on the membrane. The probe laser deflection is determined by the membrane local slope. A geometrical optics reconstruction links the photodetector signal to the laser beam angular deviation $\Delta\Theta$, and therefore to the static membrane deformation ΔL^{ss}. Considering the membrane motion in the fundamental oscillation mode we obtain $\Delta L^{ss} \approx 0.5\Delta\Theta$ with membrane local displacement in nm and angle in μrad units. The thermal noise deformation is $\approx$10 pm.

We determine the membrane oscillation frequency by modulating the input laser power at different frequencies and applying a lock-in detection to the cavity transmitted light. At very low laser input power we identify the fundamental vibration mode around 75 kHz and higher vibration modes around 120 kHz. More precise

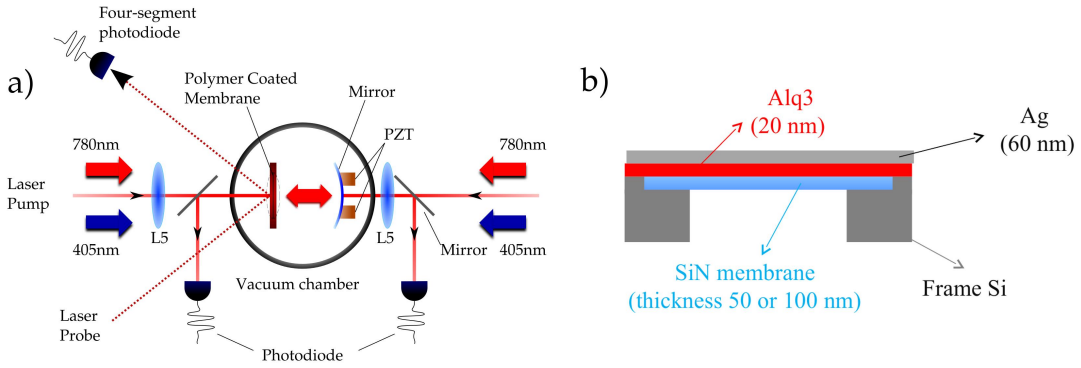

Figure 2. In a) schematics of the apparatus composed by the cavity with injection from both sides of the 780 and 405 nm lasers. A scanning of the He-Ne laser probe reflected by the membrane and detected on the four-segment photodiode produces a topographic reconstruction of the membrane deformation. In b) scheme of the membrane layers. The Ag layer represents the cavity termination, with the Alq_3 material placed inside the optical cavity.

Table 1. Optical and optomechanical parameters for the explored experimental configurations: laser wavelength, L or R configuration, experimental displacements ΔL^{ss}, theoretical displacement estimates based on the presence of radiative forces only (both in pm), radiative $c^{\rm rad}$ coefficients, bolometric $c^{\rm bol}$ coefficients, bolometric total parameter Λ^{tot}, A^{Ag} absorption within the Silver layer and $A^{\rm Alq3}$ within the Alq_3 layer, and TA total membrane absorption. The displacements are scaled to a 1 mW input power supposing a linear dependence on laser power. The Λ^{tot} signs are determined by the laser cooling occurrence on the blue frequency side and have a 30 percent indetermination.

Membrane coating	λ (nm)	L or R	ΔL^{ss}(pm) Exp	ΔL^{ss}(pm) Theo	$c^{\rm rad}_{R/L}$	$c^{\rm bol}_{R/L}$	Λ^{tot}	$A^{\rm Ag}$	$A^{\rm Alq3}$	TA
Ag only	780	R	2300	0.207	0.262	0.283	-1×10^4	0.029	0.	0.029
	405	R	3000	0.069	0.530	0.212	-1.1×10^5	0.117	0.	0.117
Alq^3 and Ag	780	R	1100	0.210	0.231	0.442	-2.7×10^3	0.031	5E-5	0.031
	780	L	1000	0.039	0.044	0.074	-1.6×10^4	0.101	0.006	0.107
	405	R	640	0.076	0.240	0.275	-7.3×10^3	0.101	0.002	0.103

determinations are obtained using the ring-down technique, where the cavity steady state is modified by applying a pulse to the input power, and the steady-state recovery takes place with oscillations at the ω_M^{eff} membrane frequency with the γ_M^{eff} damping rate. The oscillation Fourier transform allows us to determine the oscillation frequency with a 10 Hz accuracy.

4. MEMBRANE OPTICAL CHARACTERIZATION

The optical transfer-matrix method allows us to calculate the reflection and transmission coefficients of the membrane. For a multilayer medium, we must specify the incident side on the membrane: as discussed in[16] while the transmittance is the same in both cases, the reflectance and absorbance can be different. Optical parameters are the complex refractive indexes of the materials. We use refractive index values from[17] for Silver, from[18] for Si_3N_4, and from[6] for as-deposited Alq_3. The predicted finesse values are 28 for the 405 nm radiation, and 77 for the 780 nm radiation, respectively, which well agree with measurements taking into account: 1) the ten percent accuracy in our measurements; 2) the large dispersion for the refractive index values reported in literature of the different materials; 3) the eventual inhomogeneities in the multilayer fabrication.

The membrane optical parameters determine also the $c^{\rm rad,bol}_{L,R}$ parameters through simple modelling as presented in the Appendix. The sixth and seventh column of Table 1 contain their values. The absorption parameters, for Ag and Alq_3 separately and for the bilayer system, are presented in the last columns of that Table.

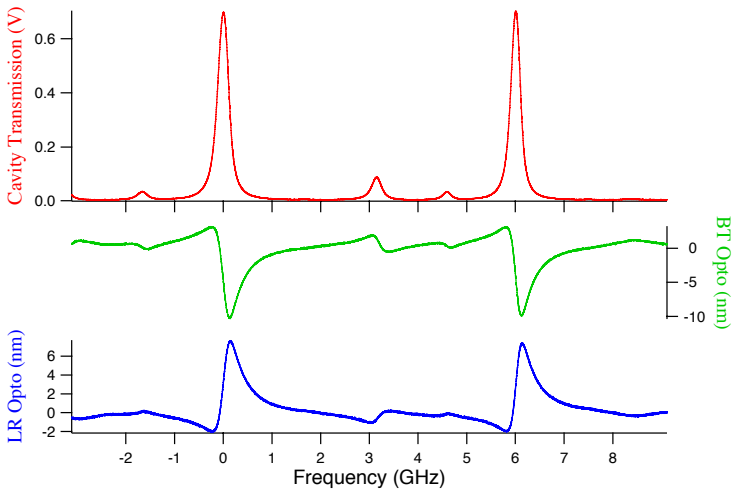

Figure 3. Cavity transmission (on the top) and optomechanical signals, BT on center, and LR on bottom, all in arbitrary units, vs. frequency detuning from the cavity resonance. Cavity transmission and optomechanical signals are observed for excitation on both the cavity fundamental mode (frequencies of 0 and 6 GHz) and the secondary ones (frequencies around 3.2 and 4.6 GHz). Observations on the Ag only coated membrane under 2.72 mW laser irradiation at 780 nm.

5. EXPERIMENTAL RESULTS

5.1 Static optomechanical signals

The detection of the static optomechanical deformation produces signals as those presented in Fig. 3, on the cavity transmission (top plot), on the left-right (LR) direction of the four-quadrant detector (central plot) and on bottom-top (BT) detection direction (bottom plot). Scanning the cavity frequency the optomechanical signals are observed for the input laser in resonance with different cavity modes. The signals for the fundamental cavity mode and for the higher cavity modes have the same shape for a given position probed on the membrane, but their sign and lineshape change. It should be pointed out that the displacements reported in Fig. 3 are to be considered only as an order of magnitude, because the optomechanical signal depends on the location of the probe laser within the membrane. Only topographic reconstructions as those presented in the following produce a more precise determination of the displacement.

The amplitude of the optomechanics displacements measured with the split-photodiode are reported within the fourth column of Table 1 for different cavity configurations. Under 780 nm radiation optomechanical signals for both right and left configurations are explored for the Alq_3-coated membrane. The fifth column reports the theoretical predictions of displacements obtained for radiation pressure forces only using Eq. (6) and the c^{rad} values of the sixth column. The measured displacements are several orders of magnitudes larger than the radiation pressure predictions. Neglecting the contribution of the radiative forces, and inverting Eq. (6) while using the c^{bol} of the seventh column, we derive the experimental photothermal Λ^{tot} parameters (including both Ag and Alq_3 contributions) reported within the Table eighth column. Only amplitudes, and not signs, are derived or Λ^{tot} from the static optomechanical signals.

5.2 Static topographic reconstruction

The measured topographic reconstruction of the membrane displacement is shown in Fig. 4a), with the L-R optomechanical signal plotted vs the (x, y) probe position on the membrane. The plotted surface is an interpolation between the measured points. The detected optomechanical signal is proportional to the local derivative of the membrane displacement. Therefore the experimental signal should be compared with the membrane deformation associated to different vibration modes. Supposing the signal produced by the fundamental acoustic mode of the membrane, we predict the signal spatial distribution shown in Fig. 4b). The comparison between experimental and theoretical signals evidences the main contribution by that membrane vibration mode to the observed signal.

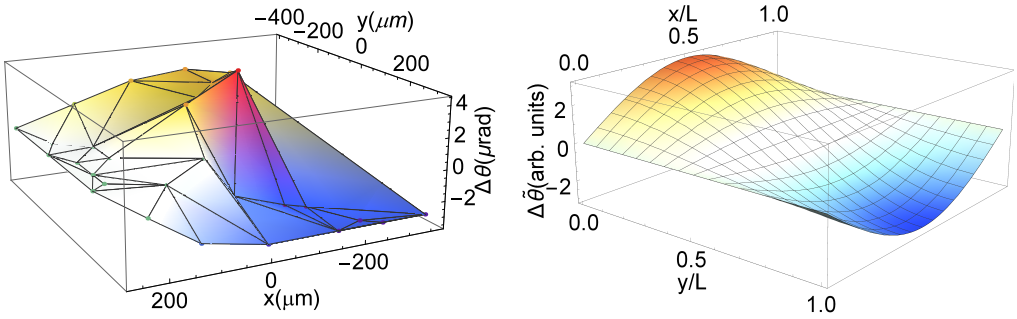

Figure 4. Topographic reconstruction of the static optomechanical membrane response. On the left the measured probe laser angular deflection $\Delta\Theta$ in μrad vs the (x, y) laser probe position scanned over the 100 μm×100 μm membrane. On the right the $\Delta\Theta$ theoretical prediction for a membrane vibrating on the fundamental acoustic mode vs the (x, y) membrane position normalized to the L membrane dimension.

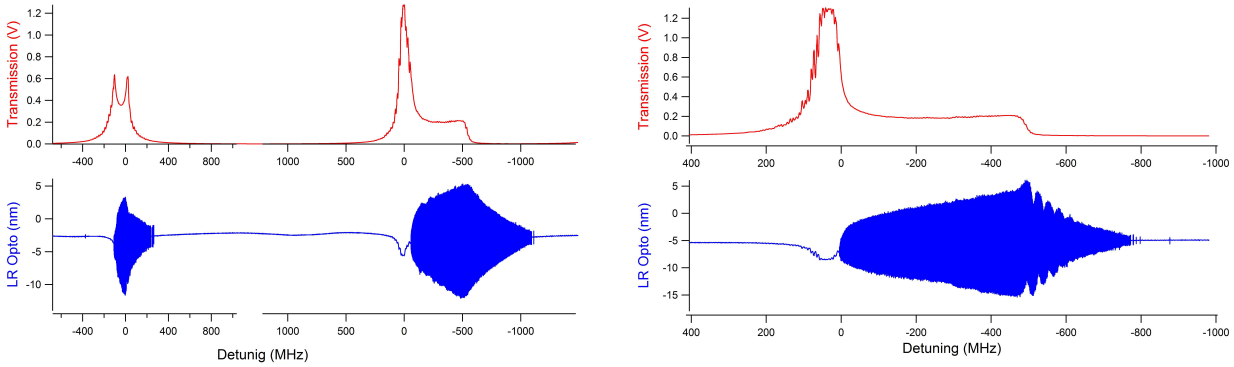

Figure 5. Membrane self-oscillation regime monitored through cavity transmission (red top traces), and through LR optomechanical signals (blue bottom traces) vs the cavity frequency detuning at $P_{in} = 1.05(1)$ mW. The left figure corresponds to a wide frequency scan from the red to the blue side of the cavity resonance and viceversa, over a 5 s total scanning time. The right figure reports the same blue-red scanning at a lower scan rate. Notice the occurrence of a detuning bistability for the laser oscillation regime.

5.3 Membrane self-oscillations

An increase of the static applied force drives the system into the nonlinear dynamics regime. For laser frequency tuned to the red side of the cavity resonance and for P_{in} input power larger than 50 μW, the self-oscillation presence is directly detected on the optomechanical signal as in the bottom records of Fig. 5 for a slow scanning of the laser frequency over the cavity resonance. A Fourier analysis of the signal reveals oscillations at the membrane free oscillation frequency, in agreement with the prediction of Eq. (7). Also the cavity laser transmission is modified by the presence of oscillations with large amplitude, as shown in the top records of Fig. 5. Scanning the input laser frequency, the self-oscillation regime is reached at different cavity detunings by inverting the red/blue directions, an evidence of optical bistability. In the left top record of Fig. 5, upon scanning from blue to red detunings the cavity transmission appears locked to a sort of metastable state with intermediate transmitted power. At larger laser detunings the standard low transmission regime is recovered. By scanning the cavity and reaching the blue detuning side, the cooling process blocks the occurrence of the self-oscillations. The competition between cooling and self-oscillations originates the peculiar double-peak structure observed on the cavity transmission. The relative amplitude of the two peaks depends on the laser scanning rate, and for slower scan the first one (towards the red detuning) is smaller than the second one. Similar double-peak behaviours were reported in Refs.[14,19] . The finding that self-oscillations occur preferentially for red detuning confirms that the Λ^{tot} parameter has a negative value.

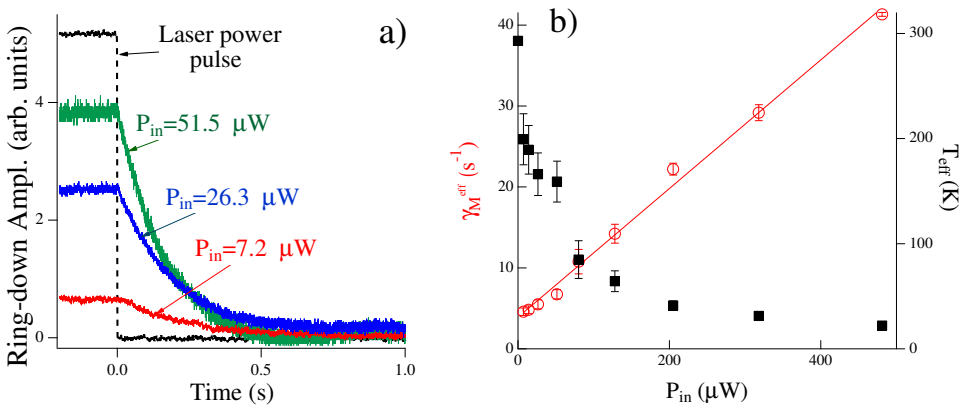

Figure 6. In (a) amplitude of the ringdown oscillations at the $\omega_M^{eff} \approx \omega_M$ frequency vs time following the switch-off of a few percent modulation to the laser input power. The black dotted line shows the temporal modulation of the laser input power. The membrane oscillation amplitude is reported for different levels of the P_{in} laser power. The exponential fit to the amplitude decrease determines the effective decay rate. In (b) effective damping rate (red circles) and effective temperature of the membrane fundamental vibration mode (black squares) of the membrane vs the cavity input power for the laser frequency tuned on the blue frequency side at one half of the cavity linewidth. The γ_M^{eff} data follow the prediction of Eq. (10a) leading to $\gamma_M/2\pi = 3.90(45)$ kHz. The effective temperature is derived from the γ_M^{eff} data using Eq. (11).

5.4 Membrane oscillation cooling

A direct detection of the membrane cooling is provided by the thermal displacement, estimated in the picometer range, smaller than our detection limit. However Eq. (11) links the cooling of the fundamental vibration mode of the membrane to the γ_M^{eff} effective damping rate and the ω_M^{eff} frequency of the membrane acoustic motion. These changes occur also for our system when the laser is tuned to the blue side of the cavity resonance. The ringdown observation measures the increase of the γ_M^{eff} effective damping with the laser power, as in the experimental results of Fig. 6a), with results indicated by the red circles in Fig. 6b). The ringdown detection evidences also the occurrence of a very small shift of the ω_M^{eff} membrane eigenfrequency by increasing the laser input power. The temperatures derived using Eq. (11) are reported in Fig. 6b), with a minimum value around 20 K. Since membrane cooling is found only for laser tuning on the blue side of the resonance, the photothermal forces behave as opposite to the radiative ones and the Λ^{tot} parameter is negative.

6. DISCUSSION AND CONCLUSION

To characterize the large bolometric forces observed in the experiment, two different parameters, Λ^{tot} and the rigidity, are introduced within the theoretical analysis of Section 2. While the initial analysis of[11] introduced the first parameter, more recent works[5,13] focused on the rigidity value. The rigidity concept describes the membrane response at the resonant oscillation frequency as in our cooling process. The rigidity may be derived from Eqs. (10) on the basis of an independent determination of the τ_c time constant, that is not available within the present investigation. The Λ^{tot} parameter determines the optomechanical static deformation, as in our topographic membrane exploration. The physics of the bolometric processes is contained within its signs and amplitudes. The sign cannot be derived directly from our topographic measurements. Instead the occurrence of the cooling process on the blue frequency side, for all the investigated membranes, evidences that the forces acting on the membrane have a sign opposite to the radiative ones, thus leading to $\Lambda^{tot} < 0$. Signals with large absolute values are observed also for excitation with the 780 nm laser, where the Alq_3 absorption is negligible, highlighting the large bolometric forces generated by the Silver coating absorption in agreement with findings by[4,9,14] . The presence of those forces is supported by the observation of optomechanical signals also for Ag-only coated membranes, and by their absence for uncoated, Si_3N_4 membranes. For comparison, in ref.[14] the factor Λ measured for a doubly sided Au-coated cantilever was -95, whereas for the cantilever coated on one side it was 4000. This last value has the same order of magnitude of our 780 nm ones, except for a sign change. Notice that

in our cavity geometry the silver mirror is on the outside of the optical cavity, while in[14] measurements is on the inside. Therefore a similar mirror deformation leads to an opposite cavity deformation.

For a given photothermal process the bolometric forces, i.e., the Λ^{tot} parameter, should be proportional to the material absorption coefficient. This proportionality is satisfied by the measurements on the Ag-only coated membrane for which the last column of Table 1 reports a larger absorption at 405 nm due to the optical interference within the Silver layer. The bolometric forces are larger for a membrane coated with Silver only, suggesting that photothermal processes in Alq_3 are associated to a different optomechanical mechanism with an opposite sign of the bolometric forces, or that the presence of the organic semiconductor modifies the Silver photothermal behaviour. For the Alq_3-coated membrane the proportionality between the TA total absorption and the Λ^{tot} parameter is not well satisfied. Such proportionality is valid under the hypothesis that the bolometric forces are originated independently by the bulk Silver and Alq_3 media, without interplay processes which might occur due to media boundaries. This assumption is weakened, however, when considering that the laser intensity distribution across the membrane depends on the propagation in the whole cavity. In fact a more general approach deriving the complete spatial dependence leads to different values for the geometrical coefficients and the absorption of each membrane layer. Such analysis also highlights that the amplitudes of the photothermal force can be controlled by fabricating membranes with different thickness of the Silver and Alq_3 layers.

In summary, we have presented the optomechanical properties of a cavity containing a multilayer membrane as mirror, composed by Silver, Alq_3, and Si_3N_4 layers. We have measured the forces on the intracavity membrane with the laser injected into the cavity from the membrane or from the mirror, and compared the results with an analysis of the optomechanical forces. For the membrane deformation we have carried out a local optical measurement and performed a topographic reconstruction. Our study has produced cooling of the oscillating motion, with self-oscillations at a frequency very close to the fundamental vibration eigenmode with a threshold for their occurrence.

APPENDIX A. RADIATIVE AND BOLOMETRIC FORCE PARAMETERS

A.1 Radiative

For an absorbing membrane the calculation of the cavity reflection and transmission requires to take into account the electric field phase shift on reflection and transmission from each membrane layer. For a multilayer film as our membrane, reflection coefficients on the left and on the right sides are different, as well as the absorptions, while the T_M membrane transmission coefficient is independent on the input side.[16] Therefore we define complex amplitude reflectances for the two sides of the membrane shown in Fig. 2b)

$$r_M^j = |r_M^j| e^{i\phi_M^j}, \tag{12}$$

with the ϕ_M^j electric field phase shift and $j = (\mathrm{Ag}, \mathrm{Si})$, silver and Si_3N_4, respectively, denoting the first layer for the reflected laser radiation. Two different reflection coefficients $R_M^j = |r_M^j|^2$ are obtained. For our geometry, R_M^{Si} corresponds to the reflection of the inside cavity radiation and R_M^{Ag} to the reflection of radiation entering into the cavity from outside.

The electric field propagation equations within the cavity lead to the following $c_{L,R}^{rad}$ of Eq. (4) for the L or R experimental configurations and for the case of cavity resonance:

$$\begin{aligned} c_L^{\mathrm{rad}} &= T_1 \mathcal{F} \frac{1+R_M^{\mathrm{Si}}-T_M}{2\pi\sqrt{R_1 R_M^{\mathrm{Si}}}} \\ c_R^{\mathrm{rad}} &= T_M \mathcal{F} \frac{1+R_1-R_1 T_M+2\sqrt{R_1 R_M^{\mathrm{Ag}}}\left(1-\sqrt{R_1 R_M^{\mathrm{Si}}}\right) cos(\phi_M^{\mathrm{Ag}}+\phi_M^{\mathrm{Si}})}{2\pi\sqrt{R_1 R_M^{\mathrm{Si}}}} - \frac{\pi}{2\mathcal{F}}(1+R_M^{\mathrm{Ag}}). \end{aligned} \tag{13}$$

Applying these formula to our membrane leads to the $c_{L,R}^{\mathrm{rad}}$ values reported in the sixth column of Table 1.

A.2 Bolometric

The $c_{L,R}^{\mathrm{bol}}$ coefficients**,** taking into account the contribution of both the P_1 and P_2 intracavity powers of Fig. 1 to the absorption process, are proportional to the $P_1 + P_2$ total power propagating in the membrane. By neglecting

the attenuation produced by the membrane layers by the Silver/Alq_3 absorption the electric field propagation equations lead to the following $c_{L,R}^{bol}$ of Eq. (5) for the L or R experimental configurations and for the case of cavity resonance:

$$\begin{aligned} c_L^{\mathrm{bol}} &= \mathcal{F}\frac{T_1(1+R_M^{\mathrm{Si}})}{2\pi\sqrt{R_1 R_M^{\mathrm{Si}}}}, \\ c_R^{\mathrm{bol}} &= \mathcal{F}\frac{1+R_1 T_M}{2\pi\sqrt{R_1 R_M^{\mathrm{Si}}}}. \end{aligned} \tag{14}$$

Applying these formula to our membrane leads to the $c_{L,R}^{\mathrm{bol}}$ values reported in the seventh column of Table 1.

ACKNOWLEDGMENTS

The authors acknowledge the support by the University of Pisa through the PRA-2016-47 grant.

REFERENCES

[1] Aspelmeyer, M., Kippenberg, T. J., and Marquardt, F., "Cavity optomechanics," *Rev. Mod. Phys.* **86**(4), 1391–1452 (2014).

[2] Gigan, S., Bohm, H. R., Paternostro, M., Blaser, F., Langer, G., Hertzberg, J. B., Schwab, K. C., Bauerle, D., Aspelmeyer, M., and Zeilinger, A., "Self-cooling of a micromirror by radiation pressure," *Nature* **444**, 67–70 (Nov 2006).

[3] Arcizet, O., Cohadon, P. F., Briant, T., Pinard, M., and Heidmann, A., "Radiation-pressure cooling and optomechanical instability of a micromirror," *Nature* **444**, 71–74 (Nov 2006).

[4] Metzger, C. H. and Karrai, K., "Cavity cooling of a microlever," *Nature* **432**, 1002–1005 (Dec 2004).

[5] Usami, K., Naesby, A., Bagci, T., Melholt Nielsen, B., Liu, J., Stobbe, S., Lodahl, P., and Polzik, E. S., "Optical cavity cooling of mechanical modes of a semiconductor nanomembrane," *Nat Phys* **8**, 168–172 (2012).

[6] El-Nahass, M., Farid, A., and Atta, A., "Structural and optical properties of tris(8-hydroxyquinoline) aluminum (iii) (alq3) thermal evaporated thin films," *J. Alloys Comp.* **507**(1), 112 – 119 (2010).

[7] Kozlov, V. G., Bulovic, V., Burrows, P. E., and Forrest, S. R., "Laser action in organic semiconductor waveguide and double-heterostructure devices," *Nature* **389**, 362–364 (Sept 1997).

[8] Liew, Y.-F., Zhu, F., Chua, S.-J., and Tang, J.-X., "Tris-(8-hydroxyquinoline)aluminum-modified indium tin oxide for enhancing the efficiency and reliability of organic light-emitting devices," *Applied Physics Letters* **85**(19), 4511–4513 (2004).

[9] Vogel, M., Mooser, C., Karrai, K., and Warburton, R. J., "Optically tunable mechanics of microlevers," *Applied Physics Letters* **83**(7), 1337–1339 (2003).

[10] Meystre, P., Wright, E. M., McCullen, J. D., and Vignes, E., "Theory of radiation-pressure-driven interferometers," *J. Opt. Soc. Am. B* **2**(11), 1830–1840 (1985).

[11] Metzger, C., Ludwig, M., Neuenhahn, C., Ortlieb, A., Favero, I., Karrai, K., and Marquardt, F., "Self-induced oscillations in an optomechanical system driven by bolometric backaction," *Phys. Rev. Lett.* **101**(13), 133903 (2008).

[12] Marquardt, F., Harris, J. G. E., and Girvin, S. M., "Dynamical multistability induced by radiation pressure in high-finesse micromechanical optical cavities," *Phys. Rev. Lett.* **96**(10), 103901 (2006).

[13] Barton, R. A., Storch, I. R., Adiga, V. P., Sakakibara, R., Cipriany, B. R., Ilic, B., Wang, S. P., Ong, P., McEuen, P. L., Parpia, J. M., and Craighead, H. G., "Photothermal self-oscillation and laser cooling of graphene optomechanical systems," *Nano Letters* **12**(9), 4681–4686 (2012).

[14] Metzger, C., Favero, I., Ortlieb, A., and Karrai, K., "Optical self cooling of a deformable fabry-perot cavity in the classical limit," *Phys. Rev. B* **78**(3), 035309 (2008).

[15] Cohadon, P. F., Heidmann, A., and Pinard, M., "Cooling of a mirror by radiation pressure," *Phys. Rev. Lett.* **83**(16), 3174–3177 (1999).

[16] Potton, R. J., "Reciprocity in optics," *Rep. Progr. Phys.* **67**(5), 717–754 (2004).

[17] Yang, H. U., D'Archangel, J., Sundheimer, M. L., Tucker, E., Boreman, G. D., and Raschke, M. B., "Optical dielectric function of silver," *Phys. Rev. B* **91**(23), 235137 (2015).
[18] Philipp, H. R., "Optical properties of silicon nitride," *J. Electrochim. Soc.* **120**(2), 295–300 (1973).
[19] Marino, F. and Marin, F., "Coexisting attractors and chaotic canard explosions in a slow-fast optomechanical system," *Phys. Rev. E* **87**(5), 052906 (2013).